Gluing bifurcations in optothermal nonlinear devices

R. Herrero, J. Farjas,* R. Pons,† F. Pi, and G. Orriols
Departament de Física, Universitat Autònoma de Barcelona, 08193 Bellaterra, Spain
(Received 3 November 1997)

The gluing process through which two limit cycles become a two-lobed limit cycle by involving an intermediate saddle point has been investigated in the reflection of an optothermal nonlinear device that behaves as a three-dimensional dynamical system. Sequences of both periodic and aperiodic oscillations of complex hybrid structures appear during the process. The observed phenomena have been interpreted as arising from a set of homoclinic bifurcations organized around some codimension-two global bifurcations in which the saddle point experiences homoclinicity at both sides simultaneously. Experimental results are compared with numerical simulations. [S1063-651X(98)12305-X]

PACS number(s): 05.45.+b, 42.65.Pc

I. INTRODUCTION

Local and global bifurcations are powerful tools for understanding the appearance of complex dynamics in nonlinear systems. Multiple bifurcation points appearing in the parameter space are particularly significant because they act as organizing centers of a variety of qualitatively different dynamics. Concerning local bifurcations, accurate analysis of the bifurcation set may be obtained through the normal forms derived by applying the center manifold theorem near the degenerate point. This way is really powerful because it evidences the intrinsic association of a homoclinic connection with certain degenerate local bifurcations and shows how the corresponding global bifurcation curve emerges from the codimension-two point [1,2].

Homoclinic orbits are trajectories biasymptotic to a saddle limit set both forward and backward in time, and their crucial role in the mechanisms originating chaos in dynamical systems is now widely recognized [1,3–5]. Homoclinicity is reached when the unstable and stable manifolds of the saddle approach to cross one through the other by varying some parameter and a global bifurcation affecting both sides of the saddle separatrix then occurs. During the process a number of periodic orbits may be generated (destroyed) and, according to the actual saddle configuration, complex dynamics may appear [6]. The homoclinic orbit characterizes a recurrent mechanism for global folding of phase space, while the saddle set provides stretching, folding, and contraction of the flow at a local level.

Homoclinic bifurcations of codimension higher than one are also possible. A variety of cases arise from the violation of some nondegeneracy condition affecting either the saddle eigenvalues or the twistedness of manifolds around the homoclinic orbit [7]. Typically a number of additional bifurcations of both local and global nature emerge from the degenerate point of the homoclinic bifurcation curve. More complex situations may occur when two different homoclinic bifurcations of the same saddle invariant set cross one another [8–13]. These are the so-called gluing bifurcations and the present work reports numerical and experimental results dealing with one of such bifurcation.

Gluing together two attractors is a consequence of a kind of global bifurcation during which two attractors living at the opposite sides of a saddle separatrix are destroyed and a new attractor is created occupying the loci in phase space of the previous ones. In the gluing process both branches of the saddle unstable manifold approach the separatrix and a variety of successive homoclinic connections occur through which the original attractors disappear and new periodic orbits of hybrid structure are created. In the parameter space, the gluing phenomena appear organized around the point where both branches of the saddle unstable manifold experience homoclinicity simultaneously. In the absence of symmetry, such a point describes a codimension-two global bifurcation.

Examples of transitions to chaos through gluing processes have been found in models developed in the context of the Rayleigh-Bénard convection [14], reaction-diffusion systems [15], parametrically excited surface waves [16], and magnetoconvection [17]. To our knowledge, however, experimental observations of gluing bifurcation phenomena have been reported in the literature for two-dimensional dynamical systems only [18]. In two dimensions the gluing process is simple. Only the two original limit cycles and the resulting two-lobed cycle may be involved and the possible saddle connections reduce to the four combinations between the pairs of one-dimensional branches of the stable and unstable manifolds. In three-dimensional phase spaces, however, the possibility of different homoclinic connections increases indefinitely and a large variety of hybrid periodic orbits may be created and complex dynamics may occur [10,11]. This paper describes a gluing process observed in the response of a three-dimensional dynamical system and which corresponds to the simple case of a saddle point with real eigenvalues.

This work has been done with a nonlinear optothermal device that involves a periodic nonlinearity and that, for this reason, provides an optimum situation for the achievement of gluing phenomena. Such a periodicity originates repetition of

*Present address: Departament d'Enginyeria Industrial, Universitat de Girona, Avinguda Santaló s/n, 17071 Girona, Spain.

†Present address: Departament de Física i Enginyeria Nuclear, EUETIT, Universitat Politècnica de Catalunya, C/. Colom 1 08222 Terrassa, Spain.

similar flow structures in an extended region of phase space and, in particular, it is responsible for (i) a multiple steady state solution consisting of successive saddle-node pairs of fixed points, and (ii) the occurrence of the same Hopf bifurcations on either the several nodes or the several saddles and the similar evolution of the corresponding limit cycles. In this way, phase portraits typically contain several attractors that, originated from the respective node points, appear separated by the stable manifolds of the intermediate saddle sets. In their evolution with the input light power, the attractors at both sides of a given saddle set may approach the saddle separatrix and may be then glued together. Another significant property of the nonlinear system is that its effective dynamical dimension may be chosen freely by simply modifying the device structure and in this way allowed us to study gluing phenomena in phase spaces of different dimensions. On the other hand, we dispose of a mathematical model that behaves mimetically to the experimental device and the numerical analysis is then really useful for the understanding of experimental results.

II. NONLINEAR DEVICE

The nonlinear system is based on the so-called optothermal bistability with localized absorption (BOITAL) and it has been described in detail elsewhere from both the experimental [19,20] and mathematical [21,22] points of view. We here remark on the basic mechanisms underlying the system dynamics and briefly describe essential details of both the experimental device and the model used for numerical simulations.

The BOITAL device is an interferometric cavity with a partially absorbing input mirror and a transparent multilayer spacer of alternatively opposite thermo-optic materials. It is illuminated by a laser beam and the time evolution of the reflected light power is the observed signal. Concretely, in the experimental device used in this work the cavity was spaced with a {glass–silicone [23]–glass} trilayer of thicknesses 140 μm, 70 μm, and 1 mm, respectively. Devices with silicone layers of different thicknesses were also employed in order to move within the parameter space. Thermal expansion works in the case of glass as a positive phase-shifting effect (10^{-5} K^{-1}) while the silicon produces negative shifting effects essentially due to refractive index changes (-4.7×10^{-4} K^{-1}). The cavity mirrors were a nickel-chrome film of 6 nm thickness coated on the first layer of glass and a TiO_2-SiO_2 multilayer stack coated on the rear glass layer. The dielectric mirror reflection was high (0.98 for the operating wavelength) while the metallic mirror had external and internal reflections of 0.17 and 0.23, respectively, and transmission of 0.46. The device was irradiated for the metal mirror side with a continuous-wave laser beam of 514.5 nm wavelength focused to a 0.3 mm diam spot, the reflected light was detected by means of a photodiode and the signal was digitized and stored in a computer. The incident light power is used as control parameter.

Time dynamics in BOITAL devices is exclusively based on the heat propagation from the absorbing mirror through the cavity spacer, while the light provides an instantaneous nonlinear feedback to the heat source. The light tests the spacer temperature by means of its own phase shift and transfers such information to the localized heat source by means of interference effects. Nonlinearity is due to the cavity response as a function of the round-trip phase shift, i.e., the interferometric Airy function. Competition and time delay between the optothermal contributions of the various layers to the light phase shift produce instabilities and consequent dynamical phenomena.

Under some simplifying assumptions, the BOITAL cavity with a multilayer spacer may be described by the homogeneous heat equations subject to a nonlocal and nonlinear boundary condition [21]. The linear stability analysis shows that the partial differential equation has effective dynamical dimension equal to the number of spacing layers and that it may be reduced to the following low-order model [22]

$$\frac{d\psi_j}{dt}=-\sum_{i=1}^{N} b_{ji}[\psi_i-a_iA(\psi)\psi_E],\quad j=1,2,...,N, \tag{1a}$$

with

$$\psi=\psi^0+\sum_{1}^{N}\psi_j, \tag{1b}$$

where ψ describes the round-trip phase shift of the cavity, ψ^0 is the phase shift in the absence of laser heating, ψ_j denotes the variation due to temperature changes of the phase shift associated with the jth layer, N is the number of layers, and ψ_E represents the incident light intensity normalized in such a way that $\Sigma a_i=1$. Expressions for the coefficients b_{ji} and a_i as a function of the physical parameters are given in [22]. $A(\psi)$ describes the input mirror absorption by including interference effects and its expression as a function of the mirror parameters is given in [21]. $A(\psi)$ is a periodic function with successive maxima and minima and it constitutes the nonlinearity of the system. A canonical form of Eqs. (1) based on the companion form matrix has been also derived [22]. The response of the system is given by the interferometer reflection $R(\psi)$ [21].

The partial differential equations and the reduced model have identical steady state solution with nearly the same linear stability behavior and exhibit very similar dynamics, at least within parameter ranges corresponding to physical devices [22]. Numerical simulations presented in this work have been done with the reduced model of Eqs. (1). On the other hand, a variety of experimental results in good agreement with numerical simulations have been already reported for BOITAL devices with one- [24], two- [18], and three- [19,20] spacing layers.

Let us briefly give a generic overview of the N-layer BOITAL dynamics in the $(\psi_1,\ldots,\psi_N)$ phase space, where the $\psi=$const hyperplanes underlie a certain repetition of flow structures as a consequence of the $A(\psi)$ periodicity. The steady state solution consists of a number of saddle-node pairs, S_m and N_{m+1}, $m=1,2,...$, added to the initial node point, N_1, through successive saddle-node bifurcations occurring by increasing the input power ψ_E. The fixed points appear aligned in a given direction determined by the cavity spacer properties, but the number of points and their ψ values depend on the cavity mirrors and the ψ_E value only. The phase portrait evolution as a function of the control parameter ψ_E is typically as follows: a limit cycle born from the

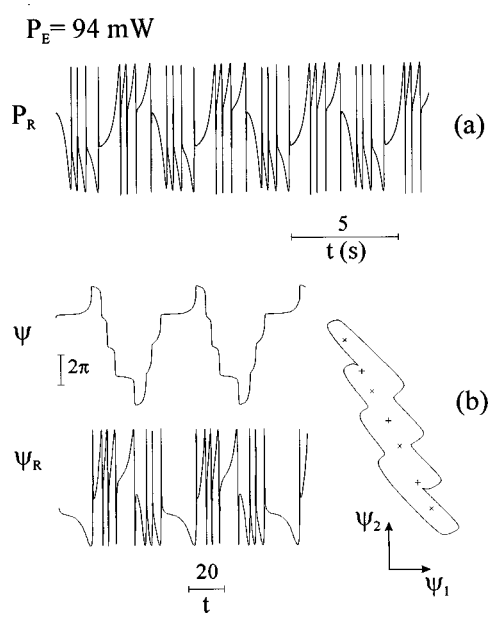

FIG. 1. Four-lobed limit cycle observed in the reflection of a BOITAL bilayer system. Experimental (a) and numerical (b) results.

N_m point is growing under the presence of a neighboring saddle set and eventually bifurcates towards more or less complex structures according to the saddle configuration. The coexistence of several limit cycles, originated from different node points, may lead to complex structures based on multiple-lobed orbits arising from gluing processes.

For $N=2$, the dynamics remains in a plane and the relevant features reduce to a variety of homoclinic bifurcations occurring when the growing limit cycles make tangency to the neighboring saddle points and either disappear or become glued to other cycles [18]. Figure 1 points out how high the gluing capability of BOITAL systems in the two-dimensional case may be. The time evolution of Fig. 1(a) was experimentally obtained from a {glass-optical gel [25]} bilayer with thicknesses of 400 and 200 μm, respectively. The evolution corresponds to a four-lobed limit cycle arising from successive gluing of four limit cycles. The numerical results shown in Fig. 1(b) illustrate the same type of attractor in both the time domain and the (ψ_1,ψ_2) phase space. The time evolutions describe both the interferometric phase ψ and the normalized reflected power ψ_R. The $\psi(t)$ signal provides the simplest picture of the evolution while the supplementary foldings on the ψ_R signal arise from interference effects and have no dynamical significance. The phase portrait shows how the limit cycle rounds around seven fixed points, of which three are saddles.

For $N=3$ the dynamics appear enriched by two things not possible in bidimensional phase spaces. First, the neighboring saddle set may be now either a saddle point with a bidimensional stable manifold or a saddle limit cycle generated by a Hopf bifurcation of that point. And second, the growing limit cycle may bend to reinject towards the inner point from which it was originated and which has become a saddle focus with outward spiraling and a one-dimensional inset. Thus, underlying the dynamics are homoclinic connections associated with saddle limit sets arising from the N_m and S_m points and having one- and two-dimensional stable manifolds, respectively. Under clear dominance of the first kind of homoclinicity the system evolution describes Rössler-type folded bands [19]. In the second case the system evolution describes Shil'nikov-type attractors if the S_m saddle is either a focus or a limit cycle [20]. In this work we deal with homoclinic phenomena associated with a S_m saddle point having purely real eigenvalues, i.e., a tridimensional saddle with a positive eigenvalue and two negative ones.

III. MAIN FEATURES OF GLUING BIFURCATION DIAGRAMS

In this section the notation is introduced and some general features of the gluing bifurcation diagrams are briefly described in order to facilitate the connection between our results and the theoretical analysis previously reported in the literature [8–13].

In symmetric systems where the homoclinic orbits at both saddle sides are necessarily simultaneous, the gluing bifurcation is achieved by varying only one parameter but in the absence of proper symmetry, as is the case in BOITAL systems, the full analysis requires good control of two parameters and the simultaneous occurrence of both homoclinic connections is a codimension-two bifurcation [8]. It has been theoretically studied for the case of a saddle fixed point with only one positive eigenvalue [10,12] and significant differences have been appreciated between the case of purely real eigenvalues and a saddle focus [10,11]. BOITAL systems may exhibit both kinds of saddle points but in this paper we consider cases with purely real eigenvalues only. In the saddle focus case the bifurcation structure is really dense and the experimental analysis becomes rather critical. Numerical simulations showing gluing phenomena associated with a saddle limit cycle have been previously reported [21] and corresponding first-return maps have been explained by means of a quite general Poincaré map model [26].

The homoclinic orbits defining the codimension-two point are denoted by Γ_0 and Γ_1, and it is assumed that independent control of both connections is provided by parameters μ_0 and μ_1, respectively, in such a way that Γ_0 (Γ_1) occurs for $\mu_0=0$ ($\mu_1=0$). It is also assumed that the corresponding periodic orbits, to be denoted by symbols 0 and 1, exist for $\mu_0<0$ and $\mu_1<0$, respectively. In the (μ_0,μ_1) parameter plane, the axes describe the principal homoclinic connections and the origin is the codimension-two point. As schematically indicated in Fig. 2, different regions can be distinguished in this parameter plane. For $\mu_0<0$ and $\mu_1<0$, both the 0 and 1 periodic orbits exist and their respective approach to the saddle point takes place as either μ_0 or μ_1 tends to 0. One of the orbits vanishes in crossing the homoclinic line while the other remains alone. In the white region within the quadrant defined by $\mu_0>0$ and $\mu_1>0$ only the 01 two-lobed periodic orbit exists. This relatively simple orbit is the final result of the gluing process but the transition taking place within the dark zones may be extremely complex. A large variety of homoclinic connections with different looping geometries of saddle manifolds can occur within the transition zones [10,11]. Each homoclinic curve creates (destroys) a new periodic orbit possessing some 0-1 hybrid structure, i.e., a trajectory moving at both sides of the saddle stable manifold and describing a certain sequence of 0 and 1

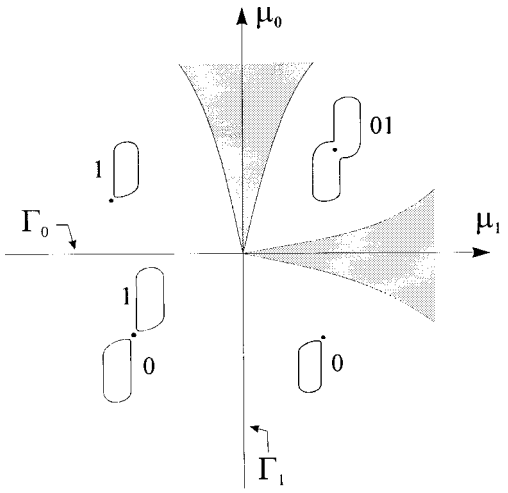

FIG. 2. Basic scheme of a gluing bifurcation in a parameter plane. Gluing processes producing hybrid periodic orbits and complex behavior may occur in the shadowed areas.

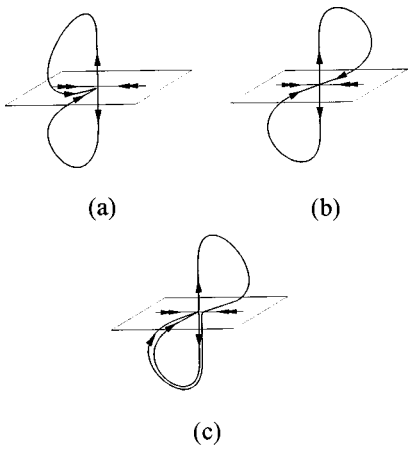

FIG. 3. Gluing configurations where the principal homoclinic orbits reach the saddle point along either the same side [(a) and (c)] or the opposite sides (b) of the strong stable manifold.

loops in a given order. The existence domain of the periodic orbit is usually limited by another homoclinic curve. The various homoclinic connections define a variety of subzones containing different periodic orbits. Superposition regions where two different periodic orbits coexist may occur in some cases according to the ordering of homoclinic curves. If two contiguous subzones do not superpose then it means that an intermediate subzone containing a different periodic orbit must exist in the middle and so on. Under some circumstances two homoclinic bifurcation curves can cross one another and then an additional global codimension-two point exists, from which more homoclinic curves emerge.

Any hybrid orbit created during the gluing process is characterized by an ordered sequence of 0's and 1's. Different sequences may be associated with the same orbit according to the starting point but different orbits have different sequences. In the considered case of a saddle having only one positive eigenvalue, it may be shown that the orbit sequences cannot contain consecutive 1's and 0's simultaneously, that no more than two periodic orbits can coexist in the same parameter domain, and that the orbits of neighboring domains are related by symbolic rules based on the Farey tree structure [10,12]. The multiple-loop homoclinic connections will be denoted as Γ_{ij}, where the first subindex indicates what kind of loop is outgoing from the saddle point while the second subindex represents the rest of the orbit sequence. The pair of homoclinic orbits limiting the domain of a periodic orbit are always of opposite beginning, i.e., Γ_{0i} and Γ_{1j} with both $0i$ and $1j$ describing the given orbit.

The actual structure of bifurcation curves around the codimension-two point depends on the form of the linearized vector field near the saddle point and the vector field geometry in the neighborhood of both Γ_0 and Γ_1 homoclinic orbits [10,11,13]. We consider the case of a saddle with purely real eigenvalues, of which only one is positive and one among the rest is lower in modulus than the others. Such eigenvalues denoted as λ_1 and $-\lambda_2$ describe the departure from and the arrival at the saddle point, respectively. Under these circumstances two kinds of situations must be distinguished according to whether the principal homoclinic orbits reach the saddle point along the same side (butterfly configuration) or opposite sides (figure eight configuration) of the strong stable manifold [10,11]. The two situations are schematically shown in Figs. 3(a) and 3(b), respectively, for a three-dimensional phase space. The basic gluing process in BOITAL systems possess the figure-eight configuration but secondary codimension-two points arising from the crossing of other homoclinic connections may be equivalent to the butterfly configuration, as shown in Fig. 3(c). On the other hand, it is also relevant to consider the kind of twisting the flow experiences along trajectories nearby the principal homoclinic orbits. Different structures of homoclinic bifurcations occur if the orientation is either preserved along both orbits, or inverted along both orbits, or preserved in one orbit but inverted in the other [10].

In two-dimensional phase spaces, the saddle point has one-dimensional manifolds. Four different saddle connections can occur and the corresponding curves cannot cross themselves except at the codimension-two point, where the invariant manifolds necessarily exhibit a figure-eight configuration. The order of the homoclinic bifurcations is necessarily like that shown in the diagram of Fig. 4(a) and it implies the coexistence of the 01 two-lobed orbit with either the 0 or 1 orbits. Nevertheless, in strongly dissipative systems like the BOITAL ones, the high negative eigenvalue with respect to the positive one is responsible for such an extreme narrowing of the coexistence regions, which makes their observation difficult. As a matter of fact, we have investigated gluing phenomena in BOITAL bilayer devices without being able to detect any superposition of orbits in the transition from single- to two-lobed orbits both experimentally [18] and numerically [22]. On the other hand, the results shown in Fig. 1 illustrate a situation in which three successive gluing processes involving different saddle points had occurred and a four-lobed periodic orbit has been created in a two-dimensional phase space.

In phase spaces of higher dimension both the saddle manifold configuration and the orientation properties of the reinjection motion are significant in determining the bifurcation diagram. As a particular example that will be useful for our analysis, we show in Fig. 4(b) the gluing bifurcation diagram for the butterfly configuration and for the semiorientable case in which orientation is preserved near Γ_1 but

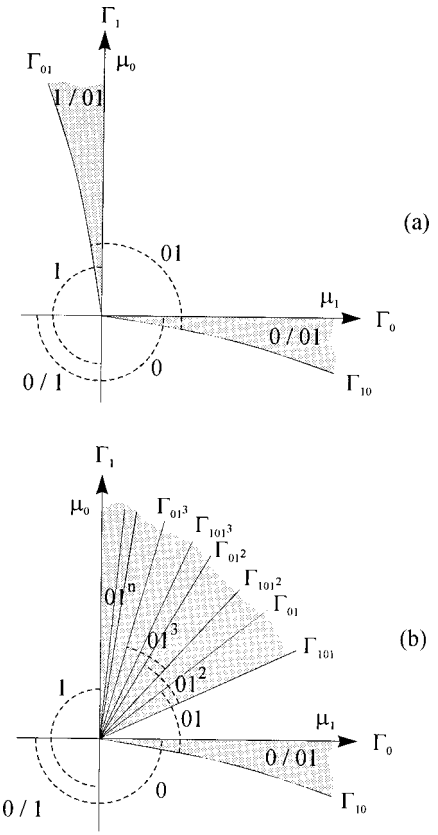

FIG. 4. Gluing bifurcation diagrams for the two-dimensional case (a) and for a three-dimensional saddle point with $\lambda_1-\lambda_2<0$ and homoclinic orbits in the butterfly configuration with orientation preserved near Γ_1 but inverted near Γ_0(b). Broken line arcs denote periodic orbit domains.

inverted near Γ_0 [10]. In this case the gluing complexity appears nearby Γ_1 only. There is an accumulation of periodic domains with orbits of type 01^n, where n indicates the number of successive 1's and it increases when approaching to Γ_1. The 01^n periodic orbit appears associated with the pair of homoclinic bifurcations $\Gamma_{101^{n-1}}$ and Γ_{01^n}. The domains of different periodic orbits appear superposed upon one another, except for the Γ_1 boundary where the accumulation of 01^n orbits takes place.

Up to now we have implicitly supposed a saddle point of negative value, i.e., the leading eigenvalues fulfill $\lambda_1-\lambda_2<0$. This is important because it means that each homoclinic connection creates a single periodic orbit that is stable [27]. In the contrary case, when $\lambda_1-\lambda_2>0$, a single periodic motion arises also from each homoclinic bifurcation but it is not stable [27]. The gluing process observed in the three-dimensional BOITAL system corresponds to a positive saddle and, for this reason, the stable periodic orbits detected in both numerical simulations and experiments must become unstable before reaching homoclinicity. This implies more complex bifurcation diagrams with additional bifurcation curves that arise from the proper codimension-two points on the homoclinic bifurcation curves. Typically, cyclic saddle-node bifurcations appear in the case of an orientation-preserving homoclinic connection while period-doubling bifurcations accompanied by homoclinic bifurcations of the period-doubled orbits will occur when the orientation is inverted [7]. Except for the case of Lorenz-like equations [29], the theoretical analysis of gluing bifurcations reported in the literature consider the negative saddle case only [8–13].

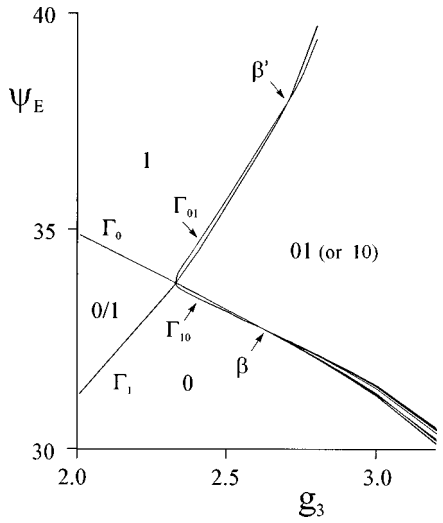

FIG. 5. Numerical bifurcation diagram for a BOITAL trilayer system, represented in the parameter plane defined by the thickness of the third layer and the input light intensity.

IV. GLUING BIFURCATION OBSERVED IN THE BOITAL SYSTEM

This section describes a numerical bifurcation diagram obtained for a BOITAL trilayer system [28]. It corresponds qualitatively to the experimentally analyzed gluing process. Some numerical simulations are also presented in the next section for comparison with the experimental results.

Figure 5 presents the main features of the bifurcation diagram in the parameter plane defined by the normalized incident power, ψ_E, and the thickness of one of the spacing layers, g_3. In the considered range of ψ_E values, the stationary solution of the system is constituted by five fixed points, N_2, S_2, N_3, S_3, and N_4. The diagram of Fig. 5 concerns limit cycles originated from N_2 and N_3 when they approach S_2 in the configuration schematically indicated in Fig. 6. The two basic cycles will be denoted by 0 and 1, respectively, and the corresponding homoclinic orbits to S_2 by Γ_0 and Γ_1. Both homoclinic connections occur simultaneously in the codimension-two point denoted by α in Fig. 5 and the scheme of Fig. 6 corresponds to the right-hand side of α. At the α point, S_2 has eigenvalues equal to -31.9, 1.1, and -0.2 and manifolds in the figure-eight configuration [Fig. 3(b)]. The homoclinic bifurcations Γ_{10} and Γ_{01} appear from α and no more homoclinic curves have been found around this point. Γ_{10} moves near Γ_0 up to cross from one to the other in a second codimension-two point that is denoted by β and from which a bundle of bifurcation curves emerges. On this point the saddle S_2 has eigenvalues equal to -26.4, 1.0, and -0.1 and its manifolds connect as shown in Fig. 3(c). Similarly, Γ_{01} moves near Γ_1 and another codimension-two point denoted by β' occurs in the crossing of both curves. The eigenvalues of the stable orbits and the analysis of flow sections in a proper Poincaré plane indicate that the orientation is preserved near the four homoclinic connections every-

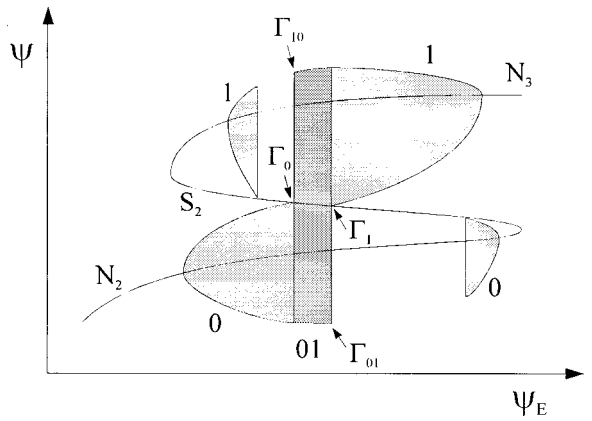

FIG. 6. Schematic bifurcation diagram as a function of the input power for a g_3 value at the right-hand side of the α codimension-two point. The order of the Γ_0 and Γ_{10} (Γ_1 and Γ_{01}) homoclinic bifurcations determines at what side of the β (β') point the system is.

where in the diagram except for the Γ_0 and Γ_1 curves at the right-hand side of the β and β' points, respectively. This indicates that the principal homoclinic orbits experience twistedness change in such codimension-two points.

We focus our analysis on the β codimension-two point and describe details of the gluing bifurcation structure found in the surroundings of the Γ_0 and Γ_{10} lines only. The basic orbits of the gluing process are now the orbits 0 and 10, where we have preferred the symbol 10 instead of the equivalent 01 in order to emphasize the opposite flow emergence from the saddle point of the two basic orbits. The main glued orbit is therefore described as 0(10). Let us also remark that in this case we are dealing with a pair of homoclinic bifurcations of a positive saddle point that involve nontwisted orbits organized in the butterfly configuration equivalent to that in Fig. 3(c) and that, after meeting together at the β point, one of the orbits (the 0) becomes twisted.

The one-parameter diagrams of Fig. 7 correspond to vertical sweepings across the homoclinic lines for three values of g_3, one located in between the α and β points and the other two at the right-hand side of β. In the diagrams we have represented the time intervals between successive passages of the orbit for a certain Poincaré plane that cuts the 0 loops only. In this way the Poincaré intersections detect both the 0 and 10 loops one time per loop only, and the 10 loops are easily distinguished from the 0 ones by their longer return times. The orbit analysis for a given ψ_E value has been done after disregarding a long enough time evolution tran-

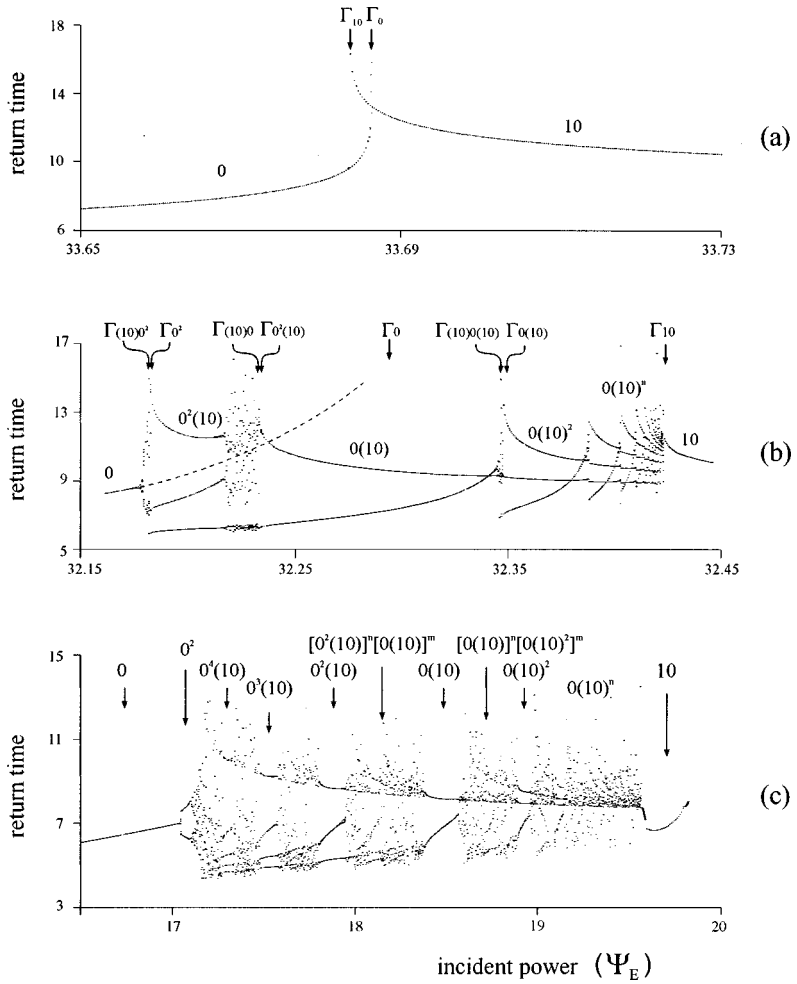

FIG. 7. Bifurcation diagrams as a function of ψ_E for $g_3=2.62$ (a), 3 (b), and 8 (c). The orbits are characterized by their return times to a Poincaré plane cutting the 0 loops only. The diagrams describe stable orbits except for the 0 saddle orbit shown by the broken line in (b) to indicate the occurrence of the Γ_0 homoclinic connection.

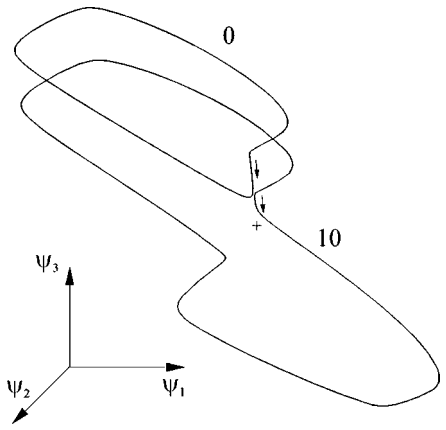

FIG. 8. Coexisting orbits for $\psi_E = 33.685$ in the case of Fig. 7(a) showing that both approach the saddle point tangent to each other. The cross denotes the saddle.

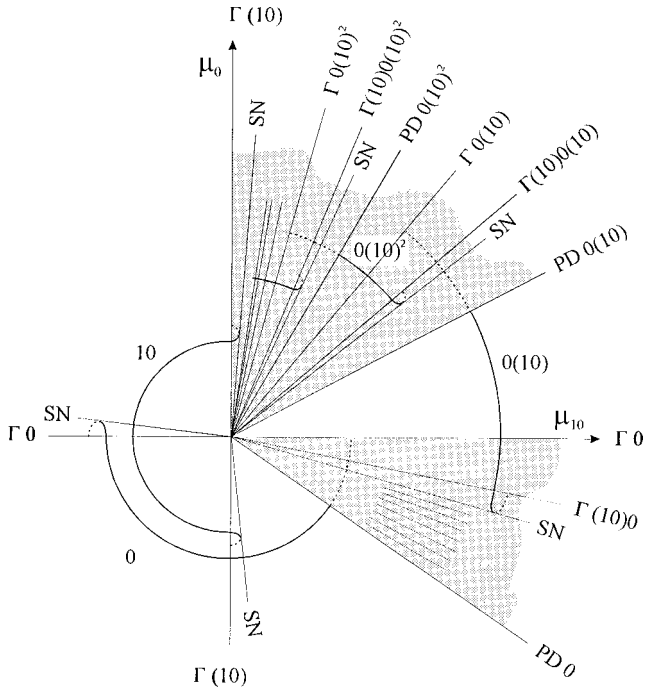

FIG. 9. Gluing bifurcation diagram corresponding to the β point. Each homoclinic bifurcation creates a saddle periodic orbit. Nontwisted homoclinic bifurcations appear in association with a saddle-node (SN) bifurcation. Twisted homoclinic bifurcations are preceded by a period-doubling (PD) sequence.

sient so that attracting orbits are solely considered. Significant stable and unstable periodic orbits have been followed by continuation techniques and characterized in detail. The windows with a discrete number of branches denote stable periodic orbits and the structure of such orbits in 0 and 10 loops is given by the number of short and long return times, respectively. When both kinds of loops appear more than one time the sequential order can be only determined by inspection of the time evolution. Asymptotic return time rises of certain loops indicate a close approach of such loops to the saddle point and the consequent vanishing of the periodic orbit suggests the occurrence of a homoclinic bifurcation. Notice that the asymptotic rises correspond to 0 loops at the right-hand side of the windows and to 10 loops at the other side. Windows with a continuous spread of points describe aperiodic evolutions and usually contain smaller periodic windows. Nonperiodic windows appear through a period-doubling sequence beginning from the previous periodic orbit and vanishes with intermittencies towards the next periodic orbit. Aperiodic evolutions are typically observed as hesitations among neighboring periodic orbits. The way the period-doubling bifurcations appear in the return time diagrams indicates that the two loops of the doubled orbit exhibit oppositely varying return time. Such a behavior is explained by noting that the doubling orbit is in the way of homoclinicity and by assuming that the two loops move oppositely with respect to the saddle point.

Consider first the diagram of Fig. 7(a) corresponding to the left-hand side of β. Only the two basic orbits 0 and 10 have been detected in this case and they appear superposed in a certain ψ_E domain. Figure 8 shows the coexisting orbits in the (ψ_1, ψ_2, ψ_3) phase space and points out how the trajectories approach the saddle in the butterfly-equivalent configuration. The two orbits vanish with an asymptotic increase of their periods in what seems the two principal homoclinicities, Γ_0 and Γ_{10}. The process is, however, more complex because each one of the orbits possess an eigenvalue that tends to $+1$ while its period increases, instead of 0 as in a regular homoclinic connection. The situation may be interpreted according to the scheme of the resonant side-switching codimension-two bifurcation for a nontwisted homoclinic orbit [30]. We suppose that the homoclinic bifurcation takes place by creating a saddle orbit while the stable orbit is even growing in period and both orbits meet then together by vanishing in a saddle-node bifurcation. Nevertheless, our continuation techniques have not been able to catch any saddle orbit and therefore we cannot confirm the bifurcation details.

Figure 7(b) corresponds to the right-hand side of β and contains a rich variety of gluing phenomena. The principal homoclinic connections, Γ_0 and Γ_{10}, appear now in opposite order as in Fig. 7(a) and, therefore, there is no coexistence of 0 and 10 orbits but two new kinds of structures have appeared. One is equivalent to the gluing structure of Fig. 4(b) for the semiorientable case of a negative saddle point, i.e., the sequence of homoclinic bifurcations ordered as $\Gamma_{(10)0}$, Γ_0, $\Gamma_{(10)0(10)}$, $\Gamma_{0(10)}, \ldots, \Gamma_{(10)}$ and the succession of periodic windows of type $0(10)^n$ accumulating towards Γ_{10}. The second kind of structure appears at the right-hand side of each periodic window in a region opened with a period-doubling bifurcation of the given orbit and ended just at the beginning of the next periodic orbit. For the $0(10)^n$ windows, such a region appears as a narrow aperiodic window resulting from the period-doubling sequence. A wider structure appears in the case of the basic orbit 0, in which a $0^2(10)$ periodic window may be seen in the middle of two aperiodic windows both appearing through period-doubling sequences. The eigenvalue analysis points out that every stable periodic orbit suffers a reversion of twistedness across its existence domain. At the left-hand side, the orbits vanish with one eigenvalue tending to $+1$ and with asymptotically increasing period. As already discussed, it may be interpreted as a combination of a $\Gamma_{(10)j}$ nontwisted homoclinic bifurcation creating a saddle orbit and a saddle-node bifurcation vanishing the two periodic orbits [34]. On the con-

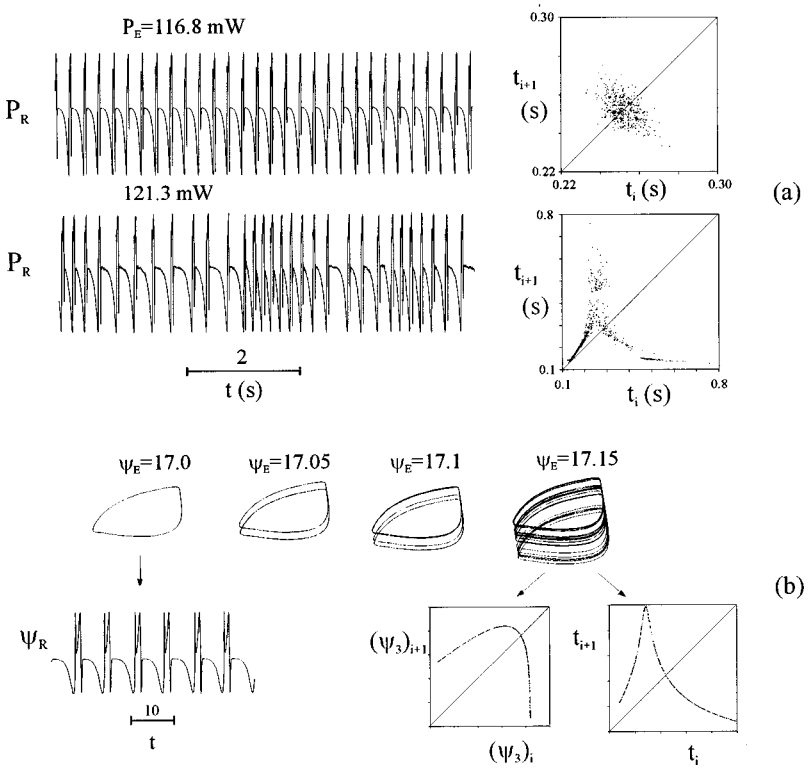

FIG. 10. Period-doubling sequence at the beginning of the gluing process. Experimental time evolutions of the reflected power and corresponding return time maps for two incident powers, (a). Numerical results showing successive phase portraits of the sequence, the time evolution of the basic 0 orbit, and return maps for the aperiodic state, (b).

trary, at the right-hand side of the windows, the orbits have an eigenvalue equal to -1 and are therefore fully twisted. A period-doubling bifurcation takes place and the remaining saddle orbit continues the asymptotic time increase towards what seems a Γ_{0j} twisted homoclinic connection. Something similar happens with the successive period-doubled orbits but it cannot be appreciated in the bifurcation diagrams, where only the 0 saddle orbit has been represented. Such behavior is clearly related with the positive value of the saddle point and the consequent fact that its homoclinic connections cannot produce stable orbits. In summary, we conclude that the main bifurcation structure around the β point is as schematically shown in Fig. 9. All of the bifurcation curves emerge from β except for the principal homoclinic bifurcations and the saddle-node bifurcation associated with Γ_{10}. The domain of a given stable periodic orbit is denoted by a solid line arc that becomes broken at the period-doubling bifurcation. Period-doubling sequences yielding aperiodic evolutions occur in the regions between the period-doubling bifurcation and the saddle-node bifurcation of the next periodic window. The additional substructure existing in the case of the 0 periodic orbit will be seen in more detail in the diagram of Fig. 7(c).

Notice that the whole structure of Fig. 7(b) covers a relative ψ_E interval lower than 1%. The experimental resolution does not permit one to distinguish details of such a structure except perhaps for the intermediate periodic window. It has been necessary to go farther from β in a situation that roughly corresponds to the diagram of Fig. 7(c). The system exhibits in this case periodic orbits of both $0(10)^n$ and $0^n(10)$ types, even if organized in a different way. The appearance of $0^n(10)$ orbits, with $n=2,3,4$, can be attributed to gluing processes between orbits of type 0^n and the basic orbit 10. As will be shown in the light of the one-dimensional map describing the gluing process, the presence of 0^n with odd n numbers may be explained as due to a period-adding sequence of saddle-node bifurcations generating superstable orbits 0^n with $n \geqslant 3$. On the other hand, a relatively large packet containing orbits of type $[0^2(10)]^n[0(10)]$ appears in between the $0^2(10)$ and $0(10)$ windows. Similarly, a group of $[0(10)]^n[0(10)^2]$ orbits appears at the other side of the $0(10)$ window. Such a complex structure can be explained if additional crossings of homoclinic bifurcations have occurred. Such a kind of hybrid orbits has not been observed in the experiment and not will be considered in more detail.

V. EXPERIMENTAL RESULTS AND NUMERICAL SIMULATIONS

Figures 10–15 present a series of experimental and numerical results illustrating a variety of states observed during a gluing process of the BOITAL system for successively increasing incident powers. The experimental results were obtained with a {glass-silicone-glass} device of thicknesses 140 μm, 70 μm, and 1 mm, respectively, and the numerical simulations correspond to the one-parameter bifurcation diagram of Fig. 7(c). Poincaré sections of the attractors obtained both experimentally and numerically appear to be almost one dimensional. It denotes strong contraction due to dissipation and suggests that the main features of the dynamics might probably be well described by means of one-dimensional maps. Time evolutions appear in the figures usually accompanied by time first-return maps and, in some numerical

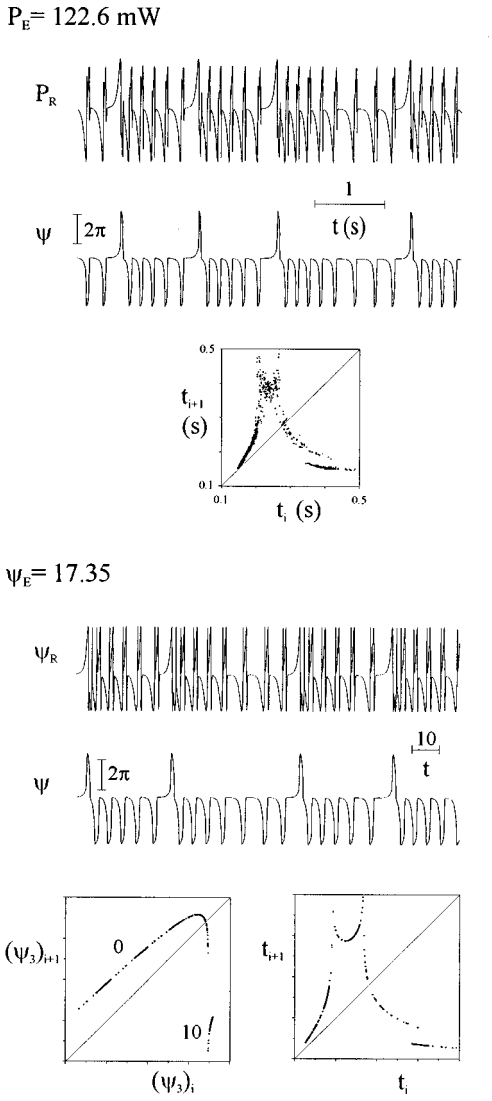

FIG. 11. Experimental ($P_E = 122.6$ mW) and numerical ($\psi_E = 17.35$) results illustrating an aperiodic orbit of type $0^n(10)$.

cases, also by return maps derived from phase-space Poincaré sections. Time maps are easily obtained from time evolutions and are particularly convenient for the experimental analysis. Time maps provide complementary information concerning time divergences but their interpretation is not immediate because each point is associated with the return

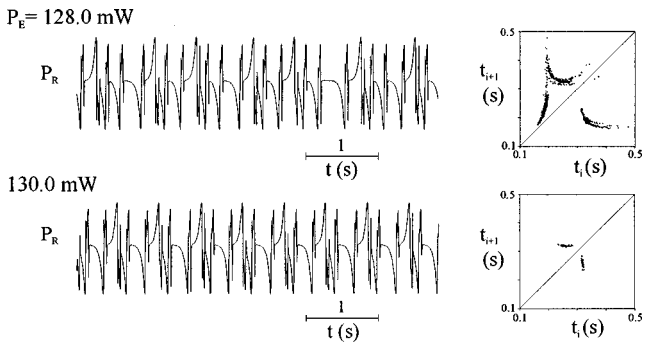

FIG. 12. Experimental results showing an aperiodic orbit of type $0^n(10)$ with n varying from 1 to 2, for $P_E = 128$ mW, and the periodic orbit 0(10) for 130 mW.

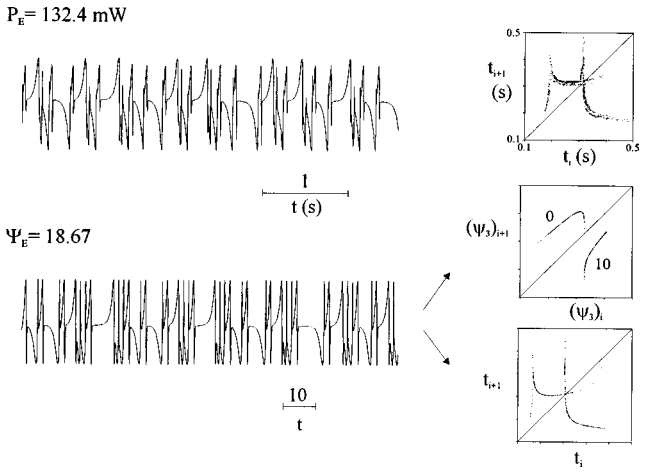

FIG. 13. Experimental ($P_E = 132.4$ mW) and numerical ($\psi_E = 18.67$) results illustrating an aperiodic orbit of type $0(10)^n$ with n varying from 1 to 2.

times of two successive loops. Phase space return maps provide a more direct interpretation of the attractor structure and will be useful for comparing with one-dimensional maps developed from the gluing bifurcation theory [31,32,13]. In all of the cases the Poincaré sections have been chosen to cut the 0 orbits of the attractors only.

Figure 10 illustrates the period-doubling sequence generated from the basic orbit 0 just before the beginning of the gluing process. The experimental evolutions correspond to the periodic orbit near the first doubling and the aperiodic state containing 0 loops only resulting from the sequence, respectively. The subharmonic process is clearly seen in the numerical phase portraits. The numerical time evolution shown in the figure represents the normalized reflected power ψ_R as a function of a dimensionless time. Such an evolution corresponds to the periodic orbit and looks really similar to the experimental one. The experimental return maps point clearly out the periodic and aperiodic behavior of the corresponding time signals. Notice that in one case the time scale of the return map is ten times longer than in the other. The agreement between the experimental and numerical return time maps is remarkable. The single hump and the shapes of both the time and phase space return maps are typical for chaotic signals arising from subharmonic cas-

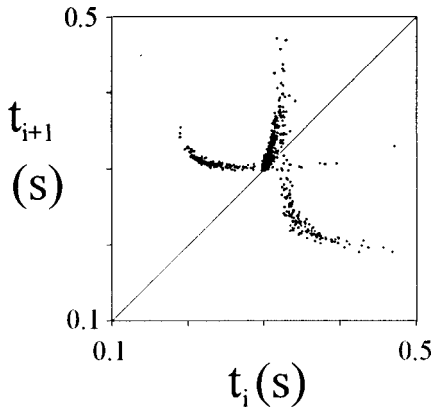

FIG. 14. Return time map corresponding to a $0(10)^n$ aperiodic orbit with n varying from 4 to 9 obtained for $P_E = 138.4$ mW.

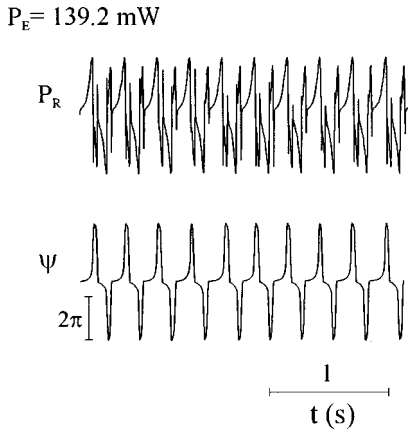

FIG. 15. Basic periodic orbit of type 10 appearing at the end of the gluing process.

cades. The stable manifold of the saddle point responsible for the gluing process lies higher than the hump of the phase space map and the iteration remains always in the 0 branch. Nevertheless, such a kind of map is able to produce superstable periodic orbits of type 0^n, with $n \geq 3$ through saddle-node bifurcations occurring when the trajectory passes for the critical point at the top of the hump [33]. These orbits experience also period-doubling sequences and, most importantly, will be involved in gluing processes with the 10 orbit when the stable manifold will touch the map hump. In this way $0^n(10)$ orbits will appear.

Figure 11 corresponds to a higher input power and shows an aperiodic hybrid orbit of the type $0^n(10)$ with n varying from 3 to 6 (from 4 to 7 in the numerical simulation). The interferometric phase $\psi(t)$ derived from the experimental signal $P_R(t)$ has been included here to point out the orbit structure more directly and to facilitate the comparison with the numerical results reported in the same figure. The time evolution points clearly out the presence of a saddle point in correspondence with the intermediate level of the signal, where the system remains a variable time interval according to how close to the stable manifold the evolution passes. The double way of departure from the intermediate level and the return to it after both kinds of departure indicate that the saddle is relatively near homoclinicity at both of its sides. Notice again the good agreement between the experimental and numerical return time maps. The well defined structure of these maps evidences the deterministic evolution of the system. The additional small branch in the lower part of both the phase space and return time maps and the return time double peak are clearly associated with the occurrence of 10 loops. The phase space map clearly points to the stable manifold of the saddle point as the vertical line to which the two branches approach tangentially. Unlike in Fig. 10, the stable manifold now cuts the top of the hump so that the trajectories passing over that manifold describe a 10 loop followed again by a sequence of 0 loops. The successive 0 loops are orientation preserving but the last one may be either nontwisted or twisted according to at what side of the critical point the iteration takes place. This means two different ways to approach the stable manifold and it is the origin of the double peak in the return time divergence. By following the return time map notice that the intersection with the diagonal describes the periodic orbit 0 and therefore the approach to Γ_0 will manifest in the displacement of this intersection point towards infinite return times. At the same time one of the time divergence peaks will approach the diagonal to merge with it at the Γ_0 homoclinicity and then the map branch will cross at the other side of the diagonal. At the same time the small lower branch will enlarge and also approach the diagonal. At a certain moment the hybrid orbit 0(10) will be created in a saddle-node bifurcation. This process is illustrated in Figs. 12 and 13. Figure 12 presents results corresponding to a $0^n(10)$ orbit, with n varying between 1 and 2, and to the periodic orbit 0(10). Notice that this periodic orbit does not necessarily lie on the diagonal since the return times of the 0 and 10 loops may be different. The return maps of Fig. 13 indicate that Γ_0 has already happened. In the phase space map, Γ_0 takes place when the periodic orbit 0 connects with the stable manifold, i.e., when the ending point of the 0 branch arrives just at the diagonal.

A qualitatively different feature has also happened in the case of Fig. 13. The 10 branch of the phase space map has surpassed the horizontal level of the stable manifold and then trajectories passing over such a level iterate again on the same branch. In this way 10 successive loops may occur as is the case in the $0(10)^n$ aperiodic orbit of Fig. 13. Two divergent peaks appear again on the return time map. The peak at the left-hand side describes passages nearby the stable manifold after having done a 0 loop while the other peak corresponds to 10 loops. The process appears more pronounced in the recording for 138.4 mW (Fig. 14), which shows a $0(10)^n$ orbit with n varying from 4 to 9. In this case the return time divergence associated with the 0 loops has almost vanished. Finally, the signal for 139.2 mW in Fig. 15 shows how the system exhibits the 10 periodic orbit at the other side of the gluing process.

The theoretical analysis of the codimension-two gluing bifurcations [31,32,13] are based on a Poincaré map that, under the assumption of a stable foliation of the return plane, can be reduced to a one-dimensional map [32]. It is not clear to what extent this condition is fulfilled in the BOITAL systems. The twofold structure clearly marked in the experimental return maps indicates that the physical devices exhibits a more complex behavior. Nevertheless the numerical return maps do not show such a twofold structure and, on the other hand, the Poincaré sections of the numerical attractors appear always as very thin curves without any sort of transverse structure. We then find it reasonable to assume that the dynamics of the BOITAL model is essentially associated with the longitudinal coordinate along the Poincaré section and that the numerical phase space return map shown in Fig. 13 provides a global overview of the one-dimensional map underlying the gluing dynamics. It is a two-branched map describing the two basic loops to be glued and with both branches ending on a common vertical line associated with the two-dimensional stable manifold of the saddle point responsible for the gluing process. The Γ_0 and Γ_{10} homoclinic connections will happen when the ending point of the respective branch reaches the diagonal. The relative position of the ending points determines at what side of the codimension-two bifurcation the system is found and, in particular, their coincidence denotes the degenerate point. It may be appreciated that in the case of Fig. 13 the Γ_0 homoclinicity has just occurred because the 0 branch appears to be just discon-

nected from the diagonal, while the Γ_{10} homoclinicity is really far. Notice also that both branches touch tangentially the vertical line so that both homoclinic connections will create a nonstable periodic orbit. This fact is related with the positive value of the saddle point. The negative (positive) slope of the 0 branch (10 branch) nearby the vertical line indicates that this part of the map inverts (preserves) the orientation of intervals, i.e., the Γ_{0j} ($\Gamma_{(10)j}$) homoclinicities involve twisted (nontwisted) connections. On the other hand, the bending of the 0 branch to acquire a positive slope permits the occurrence of stable orbits. The same happens to the 10 branch even if in this case no changes of slope sign are appreciated in the map of Fig. 13. The 10 branch will cross the diagonal before the Γ_{10} connection and a saddle-node pair of 10 periodic orbits will be then created. The saddle orbit will become the Γ_{10} homoclinic orbit while the stable orbit will be the detected state (139.2 mW signal in Fig. 15).

We consider the theoretical one-dimensional Poincaré map [32] writen as follows:

$$x_{j+1}=a_0(\mu)-b_0(\mu)|x_j|^{\xi}-c_0(\mu)|x_j|^{2\xi}+(\text{h.o.t.}),\quad x_j<0$$

$$x_{j+1}=-a_{10}(\mu)+b_{10}(\mu)x_j^{\xi}-c_{10}(\mu)x_j^{2\xi}+(\text{h.o.t.}),\quad x_j>0, \tag{2}$$

where the local coordinate x is measured on the unstable manifold, μ describes the set of parameters governing the principal homoclinic bifurcations, ''h.o.t.'' stands for ''high-order terms,'' and $\xi=-(-\lambda_2/\lambda_1)$ is the saddle index, which in our case is $\xi<1$. This means that the derivatives of the map at $x=0$ are infinite and that both homoclinic loops cannot be therefore attractive. a_0 and a_{10} characterize the separation between each one of the two branches of the unstable manifold and the stable manifold on the Poincaré plane, i.e., these parameters provide independent control of the two principal homoclinic connections. b_0 and b_{10} are the so-called separatrix quantities determining the orientation properties of the two branches of the map [31]. For the situation considered in this section, corresponding to the right-hand side of the β codimension-two point, it is $b_0<0$ and $b_{10}>0$ but at the other side of β must be $b_0>0$ in order to describe the twistedness reversion experienced by Γ_0. The second-order terms in Eq. (2) are responsible for the folding of the branches with increasing $|x|$ values necessary for permitting stable periodic orbits. Figure 16 shows a representation of the map (2) for a given set of parameters and a bifurcation diagram obtained by varying a_0 and a_{10} in such a way that both branches of the map displace simultaneously by maintaining a given separation. Similar diagrams with the same structure of main periodic windows are obtained for a relatively wide range of the map parameters. Notice also the similarities with the numerical diagram of Fig. 3(b) obtained from the BOITAL model. Nevertheless, a more careful choice of the map parameters would be required in order to reproduce the fine details appearing within the aperiodic windows. The actual shape of the map branches determines the occurrence of secondary codimension-two points in the crossing of Γ_{0j} and $\Gamma_{(10)i}$ homoclinic bifurcations and the consequent emergence of additional bifurcations [32,13].

In conclusion, complex dynamical phenomena associated with a codimension-two homoclinic bifurcation of the gluing

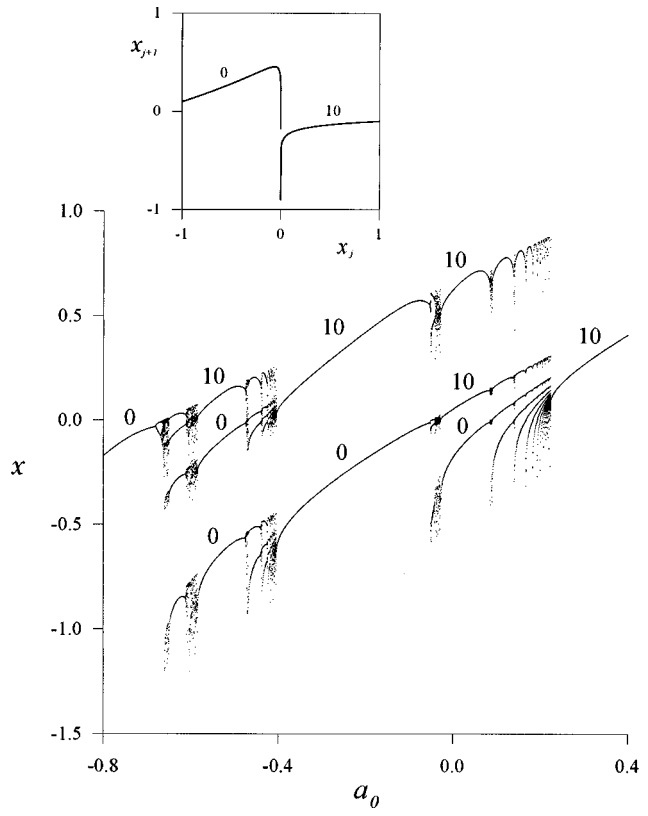

FIG. 16. Bifurcation diagram of the map (2) as a function of a_0 and for $a_{10}=a_0+0.7$, $b_0=-2.3$, $b_{10}=1.1$, $c_0=2$, $c_{10}=0.3$, and $\xi=0.2$. The inset shows the representation of the map for $a_0=-0.2$.

type have been observed in the response of an optothermal bistable device irradiated by a laser beam. A detailed analysis of a gluing transition process as a function of the input power has evidenced a variety of hybrid orbits based on combinations of the two basic periodic orbits. Return time first-return maps derived from the time evolutions have been used to understand details of the process. The clear and well defined structure of such maps confirms the occurrence of deterministic chaos in cases of aperiodic evolutions. Comparison with numerical simulations has shown a really good agreement, particularly remarkable for the return maps. The experimental analysis has been done relatively far from the codimension-two point in order to be able to observe the gluing structure in certain detail. Nevertheless, the occurrence of additional codimension-two bifurcations affecting secondary homoclinic bifurcations makes the bifurcation diagram more complex. Finally, the return maps observed both experimentally and numerically have been connected with the one-dimensional map established in the theories of the codimension-two gluing bifurcation.

ACKNOWLEDGMENTS

The authors want to thank Josep Rius for providing the experimental results shown in Fig. 1, and Marc Figueras for his collaboration in the numerical work. Financial support from the Dirección General de Enseñanza Superior, under Project No. PB96-1141, is also acknowledged.

[1] J. Gukenheimer and P. Holmes, *Nonlinear Oscillations, Dynamical Systems, and Bifurcations of Vector Fields* (Springer-Verlag, New York, 1983).
[2] P. Gaspard, Physica D **62**, 94 (1993).
[3] J. Palis and F. Takens, *Hyperbolicity and Sensitive Chaotic Dynamics at Homoclinic Bifurcations* (Cambridge University Press, Cambridge, 1993).
[4] L. P. Shil'nikov, Int. J. Bifurcation Chaos Appl. Sci. Eng. **4**, 489 (1994).
[5] P. Glendinning, in *New Directions in Dynamical Systems*, edited by T. Bedford and J. Swift (Cambridge University Press, Cambridge, 1988), p. 120.
[6] L. P. Shil'nikov, Math. USSR Sb. **10**, 91 (1970).
[7] For a synthetic review, see A. R. Champneys and Yu. A. Kuznetsov, Int. J. Bifurcation Chaos Appl. Sci. Eng. **4**, 785 (1994), and references therein.
[8] P. Coullet, J. M. Gambaudo, and C. Tresser, C. R. Acad. Sci., Ser. I: Math. **299**, 253 (1984).
[9] J. M. Gambaudo, P. A. Glendinning, and C. Tresser, C. R. Acad. Sci., Ser. I: Math. **299**, 711 (1984); J. Phys. (France) Lett. **46**, 653 (1985).
[10] D. Turaev and L. P. Shil'nikov, Sov. Math. Dokl. **34**, 397 (1987).
[11] J. M. Gambaudo, P. A. Glendinning, and C. Tresser, in *Instabilities and Nonequilibrium Structures*, edited by E. Tirapegui and D. Villarroel (Reidel, Dordrecht, 1987), p. 41.
[12] J. M. Gambaudo, P. A. Glendinning, and C. Tresser, Nonlinearity **1**, 203 (1988).
[13] D. V. Lyubimov, A. S. Pikovsky, and M. A. Zaks, *Universal Scenarios of Transitions to Chaos via Homoclinic Bifurcations*, Math. Phys. Rev. Vol. 8 (Harwood Academic, London, 1989), Pt. 4.
[14] J. Coste and N. Peyraud, Phys. Lett. **84A**, 17 (1981).
[15] Y. Kuramoto and S. Koga, Phys. Lett. **92A**, 1 (1982).
[16] E. Meron and I. Procaccia, Phys. Rev. A **35**, 4008 (1987).
[17] A. M. Rucklidge, Physica D **62**, 323 (1993).
[18] J. I. Rosell, F. Pi, F. Boixader, R. Herrero, J. Farjas, and G. Orriols, Opt. Commun. **82**, 162 (1991).
[19] R. Herrero, F. Boixader, G. Orriols, J. I. Rosell, and F. Pi, Opt. Commun. **113**, 324 (1994).
[20] R. Herrero, R. Pons, J. Farjas, F. Pi, and G. Orriols, Phys. Rev. E **53**, 5627 (1996).
[21] J. I. Rosell, J. Farjas, R. Herrero, F. Pi, and G. Orriols, Physica D **85**, 509 (1995).
[22] J. Farjas, J. I. Rosell, R. Herrero, R. Pons, F. Pi, and G. Orriols, Physica D **95**, 107 (1996).
[23] Silicone F600, from Bayer AG.
[24] G. Orriols, C. Schmidt-Iglesias, and F. Pi, Opt. Commun. **63**, 66 (1987).
[25] Gel 0608, from Cargille Lab.
[26] M. Bosch and C. Simó, Physica D **62**, 217 (1993).
[27] L. P. Shil'nikov, Math. USSR Sb. **6**, 427 (1968).
[28] According to definitions given in Ref. [17], the dimensionless parameters describing the system are $k_j = D_j = 1/0.1/1$, $\eta_j = 1/-9/1$, $g_j = 1/0.4/g_3$, for $j = 1/2/3$, $h_F = h_B = 0.5$, and cavity mirrors the same as considered in Ref. [17].
[29] V. S. Afraimovich and L. P. Shil'nikov, in *Nonlinear Dynamics and Turbulence*, edited by G. I. Barenblatt, G. Iooss, and D. D. Joseph (Pitman, Boston, 1983), p. 1.
[30] The resonant side switching occurs in the degenerate point of a homoclinic bifurcation curve where the saddle point exchanges from negative to positive value and, besides the consequent modification of the homoclinic bifurcation, a cyclic saddle-node bifurcation emerges from it [7].
[31] L. P. Shil'nikov, in the russian edition of *The Hopf Bifurcation and Its Applications*, edited by J. E. Marsden, and M. McCracken (Mir, Moscow, 1980), p. 317.
[32] J. M. Gambaudo, I. Procaccia, S. Thomae, and C. Tresser, Phys. Rev. Lett. **57**, 925 (1986).
[33] Y. S. Fan and T. R. Chay, Phys. Rev. E **51**, 1012 (1995).
[34] The $\Gamma_{(10)j}$ symbols in Fig. 7(b) indicate the occurrence of the saddle-node bifurcation while the homoclinic bifurcation takes place displaced to the right at an unknown position.